

## Østfoldbanen VL, (Ski) - Moss, Moss stasjon, Harbour, Tsunami Inundation Study

<input checked="" type="checkbox"/>	Akseptert
<input type="checkbox"/>	Akseptert m/kommentarer
<input type="checkbox"/>	Ikke akseptert (kommentert) Revider og send inn på nytt
<input type="checkbox"/>	Kun for informasjon
Sign:	

01C	For godkjenning	07.12.2021	FLo, ZL, BCa	SGI	MaR
00C	For godkjenning	12.07.2021	FLo, ZL, BCa	SGI	AKL
Revisjon	Revisjonen gjelder	Dato	Utarb. av	Kontr. av	Godkj. av
<b>Tittel:</b> Østfoldbanen VL, (Ski) - Moss, Moss stasjon, Harbour, Tsunami Inundation Study		Antall sider: <b>32</b>	<b>Entrepriise:</b>		
		Produsent:			
		Prod.tegn.nr.:		Rev.	
		Erstatning for:			
		Erstattet av:			
Prosjektnavn: Sandbukta-Moss-Såstad Prosjektnr: 960168		Dokument-/tegningsnummer: <b>SMS-20-A-59615</b>		Revisjon: <b>01C</b>	
		FDV-dokument-/tegningsnummer:		FDV-rev.:	

## INNHOLDSFORTEGNELSE

<b>SAMMENDRAG .....</b>	<b>3</b>
<b>SUMMARY .....</b>	<b>3</b>
<b>1 INTRODUCTION .....</b>	<b>5</b>
1.1 Background.....	5
1.2 Scope of work .....	5
1.3 Organisation of the report .....	5
<b>2 LANDSLIDE VOLUMES .....</b>	<b>7</b>
<b>3 LANDSLIDE RUNOUT .....</b>	<b>13</b>
3.1 Material parameters .....	13
3.1.1 Undrained strength.....	13
3.1.2 Remoulding coefficient.....	14
3.2 Scenario one.....	15
3.3 Scenario two .....	18
3.4 Scenario three.....	21
<b>4 TSUNAMI PROPAGATION AND INUNDATION .....</b>	<b>24</b>
4.1 Scenario one.....	24
4.2 Scenario two .....	26
4.3 Scenario three.....	28
<b>5 CONCLUDING REMARKS .....</b>	<b>31</b>
<b>6 REFERENCES .....</b>	<b>32</b>

## SAMMENDRAG

Det er påvist kvikkleire i et større område i Moss havn i forbindelse med planarbeidet knyttet til utbyggingen av ny jernbane og stasjon i Moss. Denne rapporten tar for seg modellering av flodbølger generert av scenarioer for store kvikkleireskred, her definert gjennom såkalte verst tenkelige hendelser. Med verst tenkelige hendelser menes her hendelser der hele eller store deler av området der det er påvist kvikkleire glir ut. Videre menes det med verst tenkelige hendelser også at hele eller store deler av skredmassene mobiliseres i løpet av relativt kort tid etter at skredet løsner. Hovedhensikten med rapporten er å etablere scenarier som underlag for beredskapsplaner i et ekstremtilfelle der et stort skred som mobiliserer hele eller store deler av den påviste kvikkleira skulle inntreffe, og deretter generere en flodbølge. Sannsynligheten for slike utglidninger av store masser med rask mobilisering er ikke vurdert i denne rapporten. De modellerte hendelsene er således ikke en del av noen risikoanalyse for området da slike analyser må inkludere de respektive sannsynligheter for hendelsene.

Modelleringen tar for seg tre ulike skredvolumer, kombinert med to ulike utløsningsområder for hvert volum, dvs. totalt seks flodbølgeberegninger. De tre ulike skredvolumene er delt i et relativt grunt scenario 1 (volum ca. 7.3 Mm<sup>3</sup>), et dypt scenario 2 (volum ca. 17.4 Mm<sup>3</sup>), og et scenario 3 der dybden på skredet ligger mellom det grunneste og det dypeste skredet (volum ca. 15.4 Mm<sup>3</sup>). For hvert av scenariene er det gjennomført beregninger både der det antas at skredet løsner i nord (nær fergekaia) og der det antas at skredet løsner lengst sør (i havneområdet). Beregningsområdet er begrenset til Værebukta samt mindre områder sør og nord for bukta. Resultatene av beregningene viser at et dypt eller midlere dypt skred kan generere flodbølger som vil gi opp mot 8 m oppskylling på Jeløya tvers over bukta for skredområdet. Resultatene viser tilsvarende oppskyllingshøyder også nær utløsningsområdet. Det grunneste skredscenarioet fører til lavere oppskyllingshøyder på opptil 3 m. Oppskyllingshøydene avtar når en kommer lenger unna skredet. Modelleringen viser videre at bølgene som genereres fra slike skred kan inntre relativt raskt, få minutter etter at skredet har startet, som betyr at det kan være lite tid til evakuering når skredet inntreffer. Videre kan skredprosessen være kompleks og mobilisere massene i flere trinn. Som følge av den kompliserte skredprosessen så vel som andre aspekter knyttet til tsunamiutbredelsen i bukta kan det oppstå flere flodbølger, og den første bølgen trenger ikke nødvendigvis være den største.

## SUMMARY

Evidence of quick clay has been found in a large area in Moss harbour in connection with the planning of a new railway and railway station in Moss. In this report, tsunami simulations are carried out for a set of large quick-clay landslide scenarios. The report presents analyses of so-called credible worst-case scenarios, which in the present report are defined as a landslide where the entire or almost the entire quick clay volume is released. In the definition of worst-case scenarios, it also follows that the quick clay masses are mobilised within a relatively short amount of time. The main aim of the report is to establish scenarios that could serve as a basis for emergency management in the extreme case where the entire volume is quickly mobilised into a landslide generating a tsunami. The report does not assess the probability of such scenarios. Hence, the simulated scenarios are presently not included in an overall risk analysis for the area as risk analysis must be associated with the corresponding probabilities of the landslide release and the subsequent run-out.

The modelling concerns three different landslide volumes, which are all combined with two different release areas, comprising altogether six different tsunami simulations. The three different landslide volumes are divided into a relatively shallow scenario 1 (volume ca 7.3 Mm<sup>3</sup>), a deep scenario 2 (volume ca 17.4 Mm<sup>3</sup>), and a scenario 3 with a depth in-between the shallow and the deep scenarios (volume ca 15.4 Mm<sup>3</sup>). Two different release areas, one in the north (near the Ferry Quay) and one in the south (in the harbour area), are used for all three volumes. The tsunami simulations are mostly

<b>BANE NOR</b> Sandbukta-Moss-Såstad	Tsunami Inundation Study	Side: 4 av 32 Dok.nr: SMS-20-A-59615 Rev.: 01C Dato 07.12.2021
--	--------------------------	---

restricted to the Værlebukta area, although smaller areas in the south and north of this bay are also included. The results of the simulations show that the two deepest scenarios generate tsunami run-up heights up to 8 m on Jøløya opposite to the landslide release area. Similar run-up heights are also found close to the release area. The shallowest scenario generates lower run-up heights up to a maximum of about 3 m. The run-up heights are gradually reduced with distance away from the landslide release area. The modelling further shows that large waves can be generated quickly, i.e., within a couple of minutes after the landslide motion has started, which implies that there can be limited time for evacuation after landslide release. Moreover, the quick-clay failure and landslide process can be complex and mobilise the masses in several steps. Consequently, due to the complexity of the landslide failure process as well as tsunami propagation and reflection, the first wave isn't necessarily the largest one.

<b>BANE NOR</b> Sandbukta-Moss-Såstad	Tsunami Inundation Study	Side: 5 av 32 Dok.nr: SMS-20-A-59615 Rev.: 01C Dato 07.12.2021
--	--------------------------	---

## 1 INTRODUCTION

### 1.1 Background

Bane NOR will build a new 10 km double track rail line from Sandbukta in the north to Såstad at Rygge in the south (Figure 1-1). The new track will include two tunnels and a new railway station in Moss. The Sandbukta-Moss-Såstad (SMS) project is part of the larger InterCity (IC) project by Bane NOR to increase train connectivity in Østlandet.

### 1.2 Scope of work

Bane NOR contracted the Norwegian Geotechnical Institute (NGI) to investigate the effect of a tsunami caused by a quick clay landslide in the Moss harbour area. NGI report SMS-00-A-590002 (NGI, 2021) evaluates the stability of the quick clay slope.

This report analyses potential landslide dynamics and tsunami generation from credible worst-case scenario quick clay slope failures. In the analysis it is assumed that the entire identified quick clay zone east of the ferry harbour area will fail. Because there is uncertainty related to the potential depth of the slope failure in such scenarios, a few different scenarios with different failure volumes are investigated. The report does not assess the probabilities for these scenarios to take place.

### 1.3 Organisation of the report

Section 2 describes the estimated landslide volumes and Section 3 outlines the landslide runout. Section 4 presents the tsunami propagation and inundation simulations due to the landslide. Section 5 provides a short conclusion.

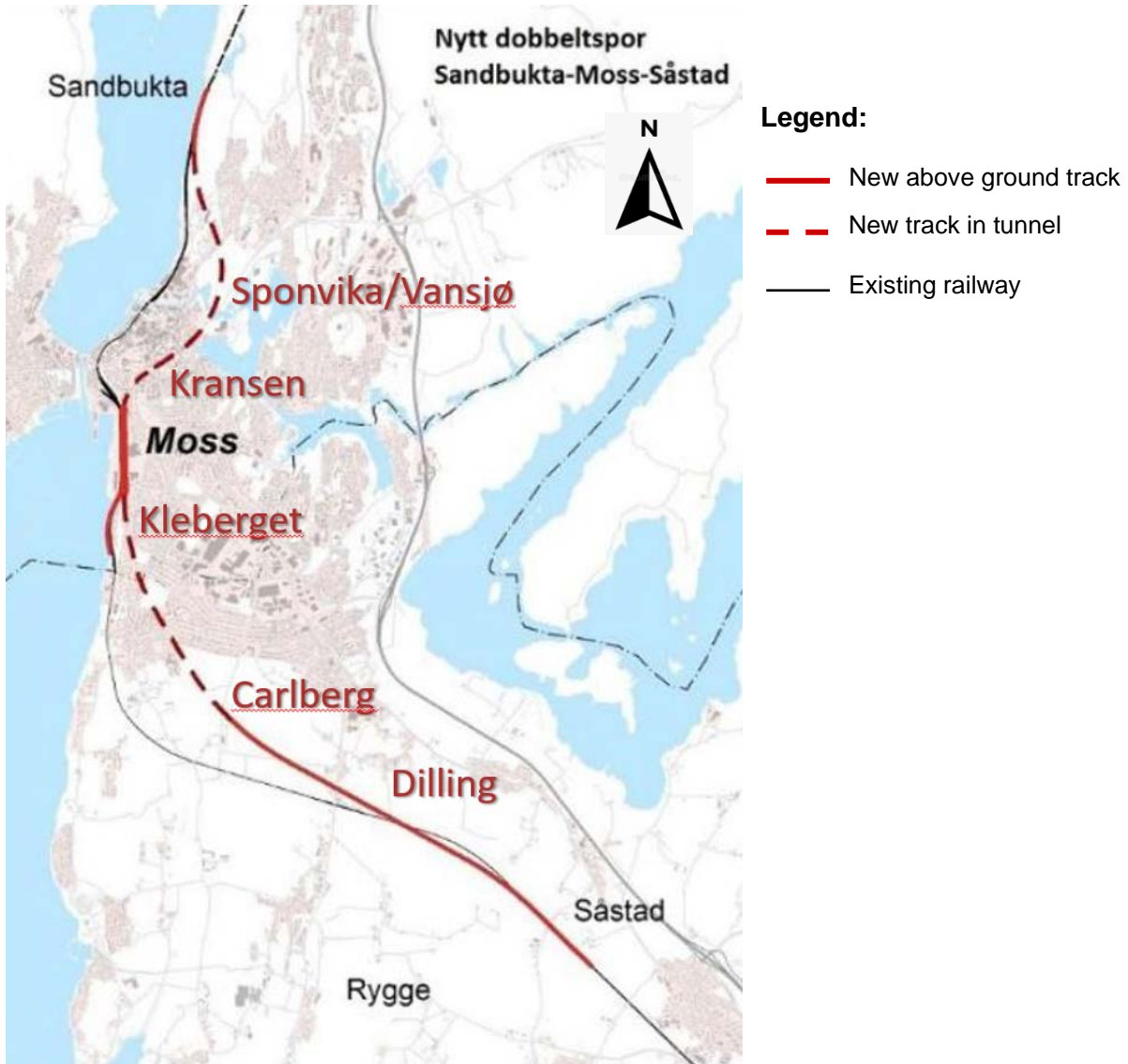


Figure 1-1 Overview map of IC SMS project.

<b>BANE NOR</b> Sandbukta-Moss-Såstad	Tsunami Inundation Study	Side: 7 av 32 Dok.nr: SMS-20-A-59615 Rev.: 01C Dato 07.12.2021
--	--------------------------	---

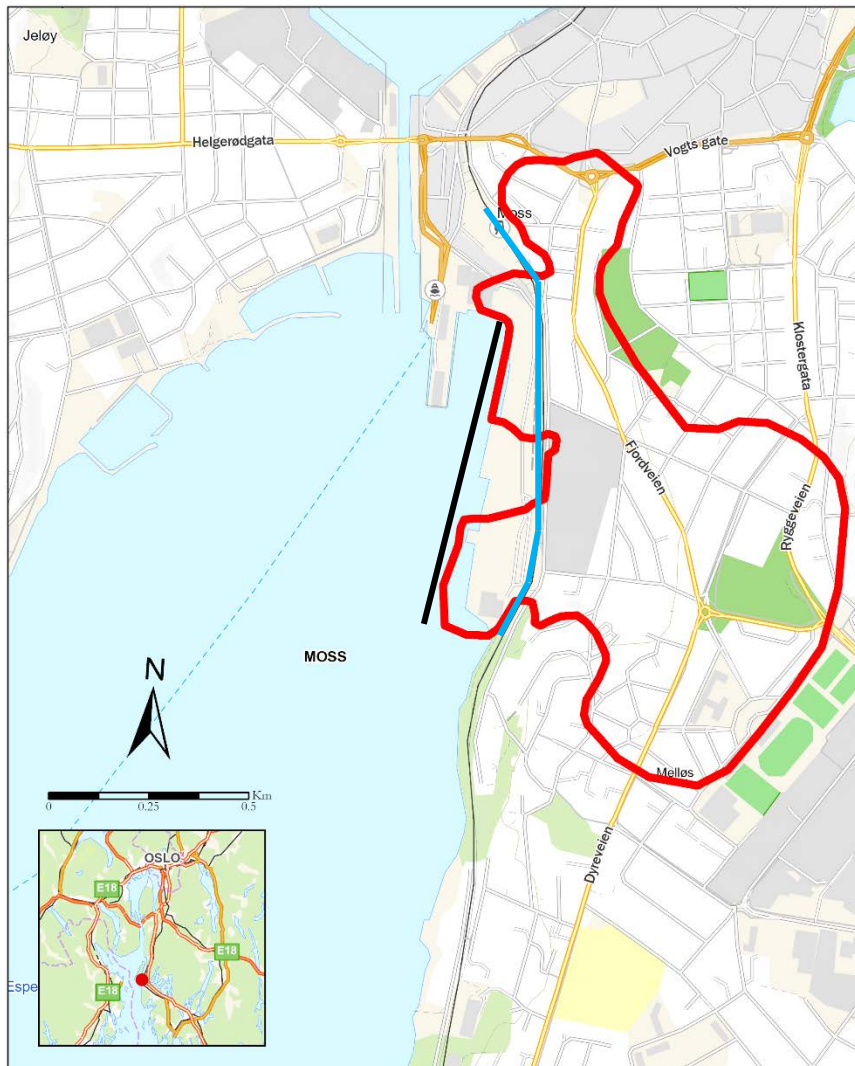
## 2 LANDSLIDE VOLUMES

Figure 2-1 shows the quick clay zone defined in NGI (2021) for the Moss harbour area. Since the calculations for this report were performed, the area where quick clay is identified has changed slightly in the upper north east corner. However, this minor change is not expected to affect the results. Mapping of the quick clay zones was based on the geotechnical site investigation according to the method described in NVE (2020). NGI assumed that the entire quick clay area fails. The depth of the soil volume that fails is uncertain. Therefore, NGI considered three different potential thicknesses of the failure volume. For each scenario, NGI assumed a failure plane with a slope of 1V:15H (NVE, 2020). For scenario one, NGI placed the foot of the slide (blue line in Figure 2-1) along the existing railway line at the bottom of the slope. For scenario two, NGI placed the foot of the slide at the bottom of the quay in Moss harbour (black line in Figure 2-1). Scenario three is the same as scenario two, except the maximum depth is limited to match better the depth of the quick clay.

Figure 2-2, Figure 2-3 and Figure 2-4 show the thicknesses of the potential failure volumes for scenario one, two, and three, respectively. For all scenarios, NGI limited the thickness of the failure volume to be less than the depth to bedrock. The thickest portions for scenario one are about 30 meters and are located near the top of the slope to the north and south. Scenario two has portions that are up to 60 meters thick at the top of the slope. Scenario two is thicker than scenario one because the foot of the failure volume is located at a lower elevation and further to the west. The failure plane extending from this location therefore cuts through more soil in the quick clay zone than the failure plane for scenario one. For the eastern portion of the quick clay zone where there is limited information on depth to bedrock, NGI restricted the thickness to be less than 20 meters for scenario one and two. Scenario three is the same as scenario two except in addition to limiting the thickness to be less than the depth to bedrock, NGI also capped the maximum slide thickness at 35 meters. In the area to the east where the depth to bedrock was uncertain, NGI limited the maximum slide thickness to 25 meters instead of 20 meters like for scenario two. This is because the quick clay is generally less than 35 meters deep, with an average largest depth of about 25 meters. In addition, the maximum depths of the failure planes calculated from the 2D slope stability analyses in NGI (2021) were only about 20 meters. Therefore, failure volumes thicker than 25 to 35 meters are not expected to occur based on the available data and experience.

The total volume of soil for scenario one is about 7.3 million cubic meters, for scenario two it is 17.4 million cubic meters, and for scenario three about 15.4 million cubic meters. For comparison, the largest quick clay slide in Norway in the 20th Century, the Rissa slide of 29 April 1978, was 5-6 million cubic meters.

NGI combined data from the client and Kartverket to develop a bathymetry/topography profile for the study area (Figure 2-5). The topography is one meter grid spacing and the bathymetry is 50 m grid spacing, except for a small section next to the Moss harbour and channel that is one meter grid spacing. NGI combined and resampled the data to 5 meter grid spacing for use in the landslide runout analyses.



**Figure 2-1 Quick clay area (red line), landslide foot scenario one (blue line) and landslide foot scenario two (black line). Inset shows location of Moss (red dot), south of Oslo.**

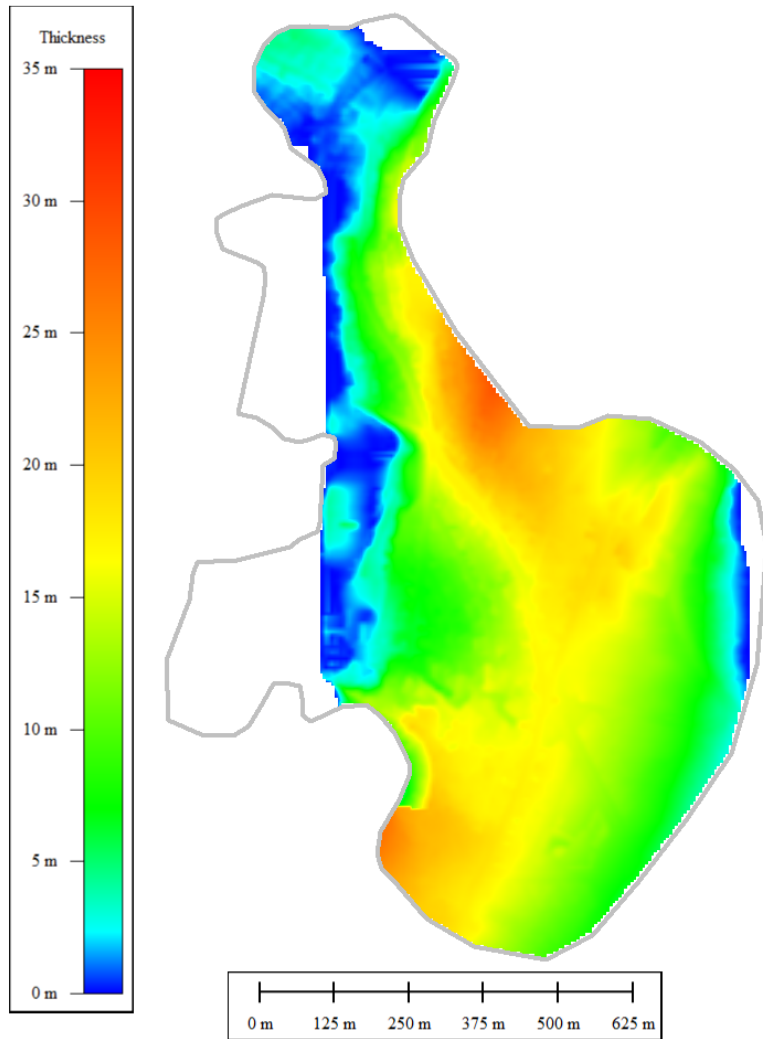


**Figure 2-2 Landslide thickness in meters for scenario one. The grey line shows the outline of the designated quick clay zone.**

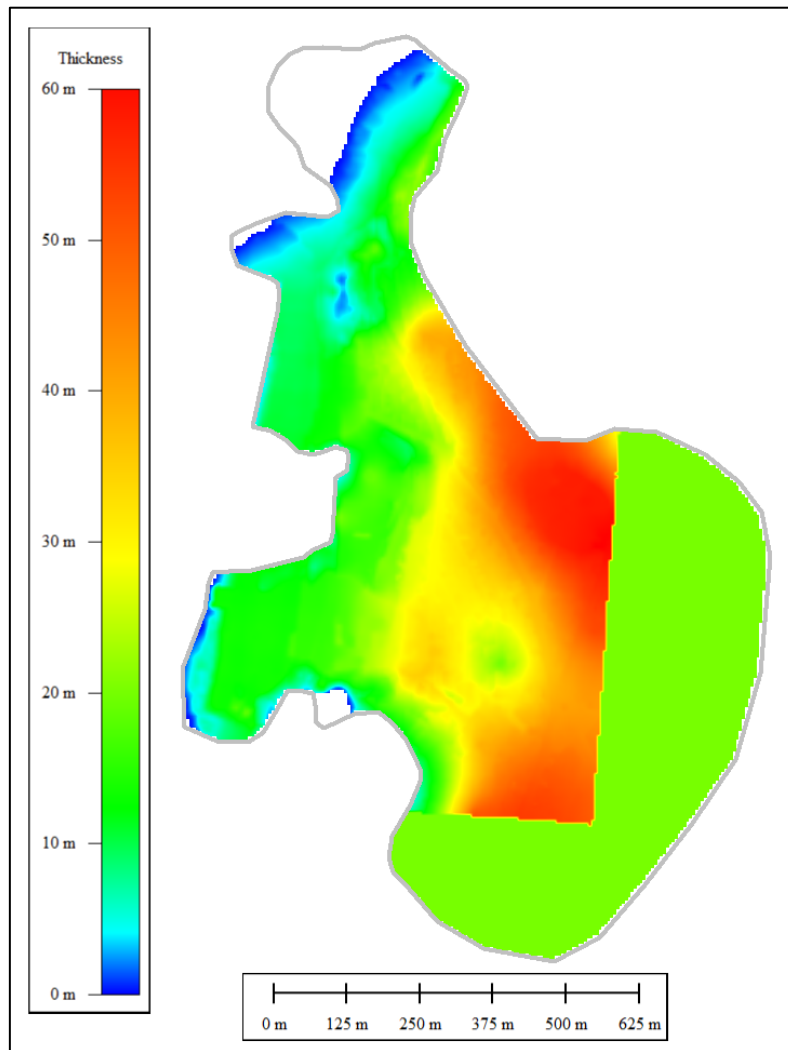
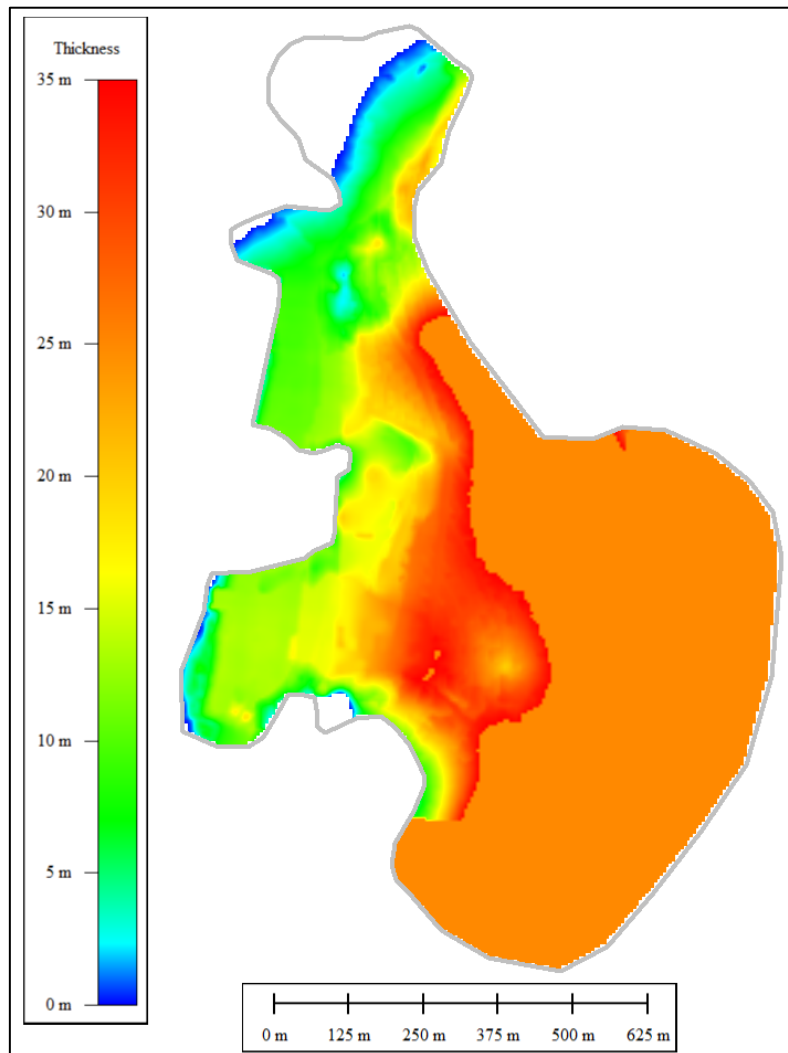
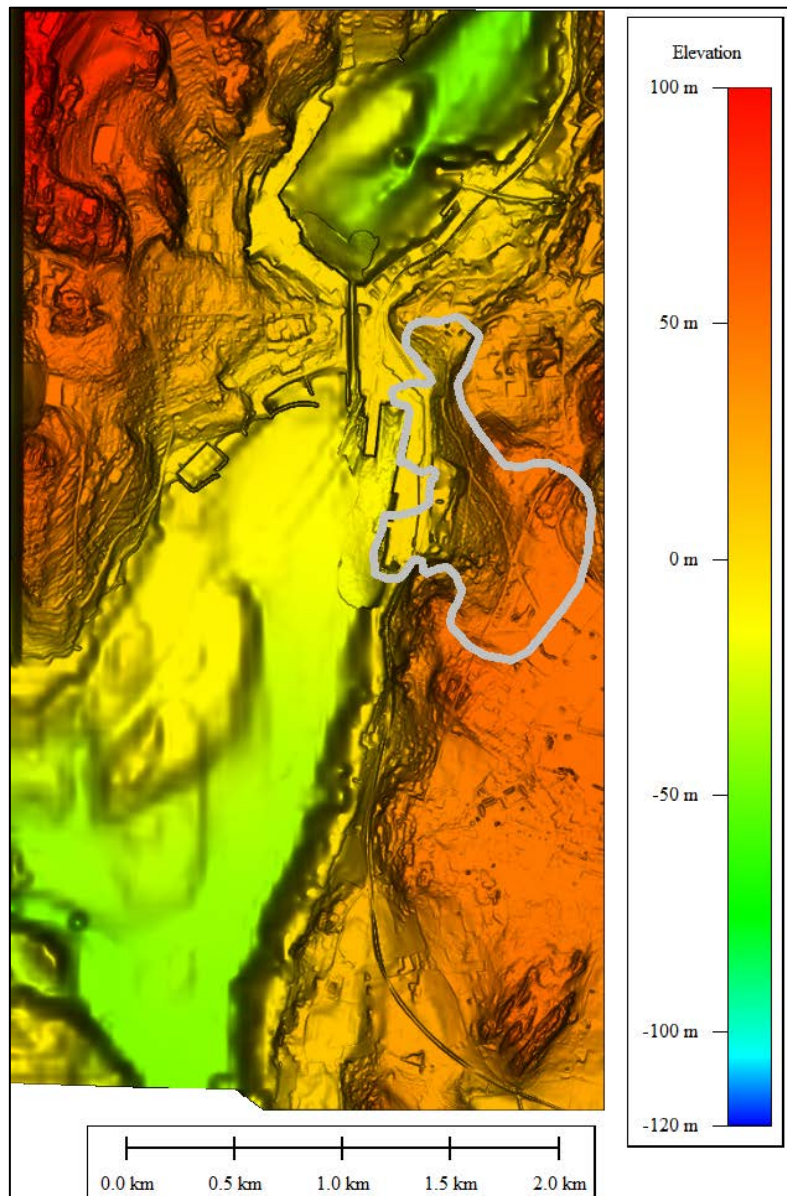


Figure 2-3 Landslide thickness in meters for scenario two. The grey line shows the outline of the designated quick clay zone.



**Figure 2-4** Landslide thickness in meters for scenario three. The grey line shows the outline of the designated quick clay zone.



**Figure 2-5 Combined topography and bathymetry. Grey outline depicts the designated quick clay zone. Bar on the right shows the elevation in m. Topography data is in NN2000 whereas the bathymetry data uses Sjøkartnull, which has a datum 61 cm lower than NN2000.**

<b>BANE NOR</b> Sandbukta-Moss-Såstad	Tsunami Inundation Study	Side: 13 av 32 Dok.nr: SMS-20-A-59615 Rev.: 01C Dato 07.12.2021
--	--------------------------	--

### 3 LANDSLIDE RUNOUT

The model BingClaw was used by NGI to calculate the landslide dynamics for the three different landslide volumes. BingClaw is a viscoplastic model developed for simulating the debris flow of cohesive materials such as clay dominated landslides, including quick clay slides (Kim et al., 2019). BingClaw embeds a feature that captures soil remoulding from intact to quick clay in a simplified manner. Remoulding is an important process for quick clay. During failure, the quick clay goes from high initial stiffness (denoted here  $\tau_{y,0}$ ) to a very low stiffness (denoted here  $\tau_{y,\infty}$ ). The remoulding feature is invoked here using the rate parameter (denoted  $\Gamma$ ) that describe how quickly the transition from intact to fully remoulded (quick) clay takes place. The remoulding allows the landslide to fail sequentially and thus mimic to some extent retrogressive failures where the slide starts the failure at the slide toe for later to progress subsequently upslope to mobilize the entire landslide mass.

The parameterisation in BingClaw for the three different landslide scenarios are described below. The related initial failure areas of these scenarios correspond to the volumes outlined in Section 2. For each of the scenarios NGI ran two independent simulations, the one first assuming that the landslide starts the failure in the northern part of the quick clay zone, the second one assuming that the landslide starts the failure development in the southern part of the quick clay zone.

#### 3.1 Material parameters

##### 3.1.1 Undrained strength

At the site, the soil profile typically consists of a 5 m thick crust and 20 m of sensitive clay overlying non-sensitive clay. The sensitivity varies from 15 to 400 between 5 and 25 m depth, based on fall cone tests in the laboratory.

The undrained shear strength ( $s_u$ ) interpreted from the piezocone test is used for the slightly overconsolidated clay in situ. Figure 3-1 shows an example design profile of  $s_u$  for the Station Area and Rockwool (Kote +0 m to +10 m) (NGI 2021). The undrained shear strength ( $s_{u,CPTU}$ ) corresponds to the undrained shear strength in triaxial compression ( $s_{uA}$ ). Yield strength  $\tau_{y,0}$  is believed to be consistent with simple shear ( $s_{u,DSS}$ ). A 35% anisotropy reduction was applied to undrained shear strength ( $s_u$ ) interpreted from the piezocone test, resulting in a depth-average undrained shear strength ( $s_{u,DSS}$ ).

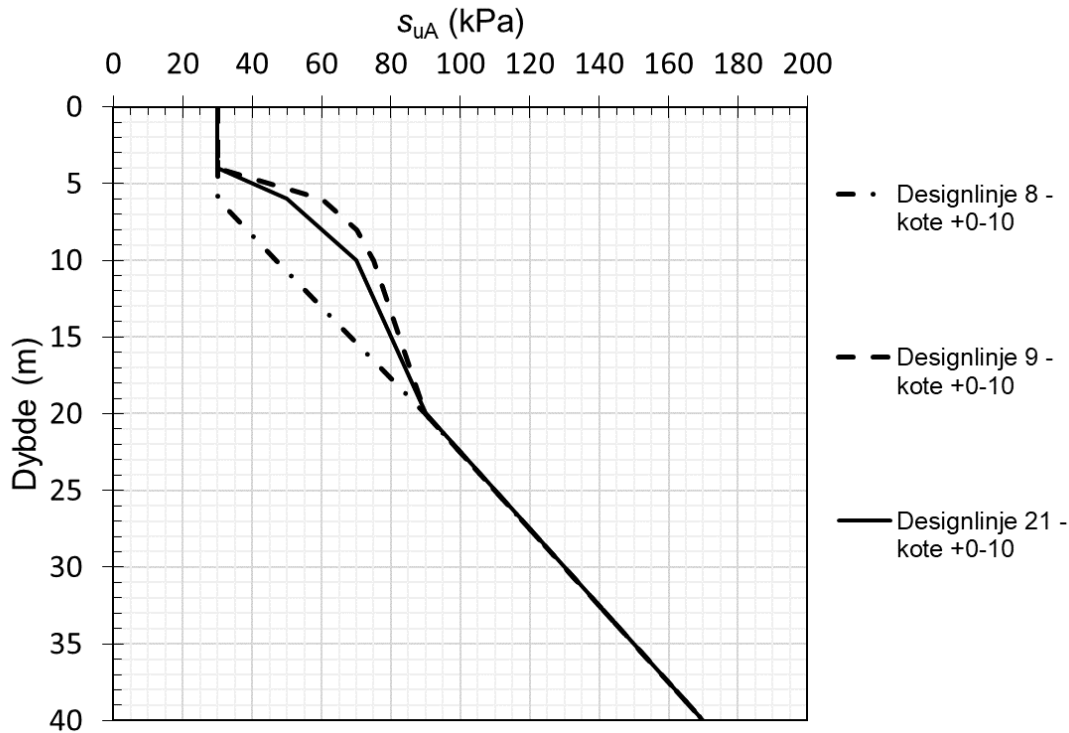


**Figure 3-1. Design profile Station Area and Rockwool (Kote +0 m to +10 m)**

For the landslide dynamics analyses, the shear strength of the clay model is depth-averaged. A single value of undrained shear strength (both intact and remolded strength) needs to be determined over the depth where the sliding takes place. The measured remolded shear strength ( $s_{ur}$ ) from the fall cone test was estimated around 3 kPa. However, the relative portion of sensitive clay decreases with depth. Hence, the remolded yield strength averaged over the soil volume will increase when the soil thickness is increased. To reflect this behavior in the scenario models, we use a 1 kPa remolded yield strength value for the shallowest failure (scenario 1), a value of 3 kPa was used for the intermediate failure (scenario three), and a value of 5 kPa was used for deeper failure (scenario two).

It should be noted that the initial strength in the model needs to be larger than the combination of gravity and depth-integrated earth pressure gradient to ensure the mass is initially at rest to reflect present day stability. To initiate the localized failure, the yield strength was set to the fully remolded value in a small failure zone either in the northern or southern part of the quick clay zone. When this initial failure zone starts to move, the remaining part of the quick clay zone will gradually lose its strength and a larger part of the zone will be mobilized as a landslide in this modelling framework.

### 3.1.2 Remoulding coefficient

Sinding-Larsen (2019) studied of the rate of remoulding coefficient,  $\Gamma$ , using the data from over 60 locations at the sites of 20 different Norwegian clays, including both sensitive and non-sensitive clays. Figure 3-2 presents Sinding-Larsen's relationships between the rate of remoulding coefficient,  $\Gamma$ , and liquidity index, peak remoulded shear strength and remoulded shear strength. A relatively high  $\Gamma$  value of 0.1 was used as an input parameter for the landslide dynamics analyses given the high peak undrained shear strength of the clays at the site. This value is used based on previous

modelling experience. The rate of remoulding coefficient  $\Gamma$  has a strong influence on the rate of remoulding of the sensitive clay and therefore the runout distance and the landslide velocity. Liu *et al.* (2018) presented additional studies on the runout distance as a function of a parametric variation of the rate of remoulding coefficient  $\Gamma$ .

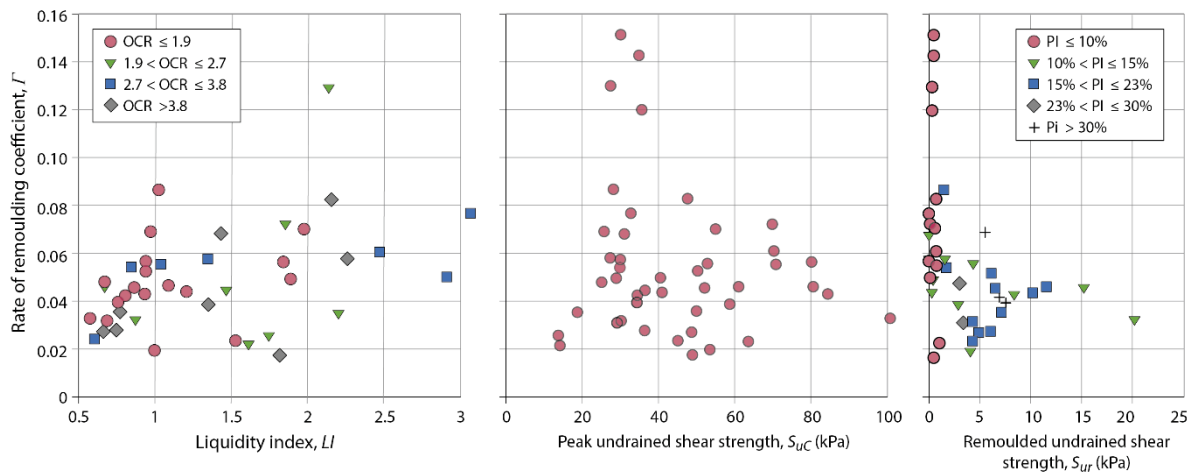


**Figure 3-2. Variation of rate of remoulding coefficient,  $\Gamma$  as a function of liquidity index, peak undrained shear strength and remoulded undrained shear strength in clays in Norway.**

### 3.2 Scenario one

This scenario represents the shallowest failure (maximum thickness is around 30 m) and the smallest volume (around 7.3 Mm<sup>3</sup>) with lower yield strength values which makes the material more mobile. This scenario uses the following yield strength parameters.

- $\tau_{y,0} = 70$  kPa, and  $\tau_{y,\infty} = 1$  kPa

Figures 3-3 and 3-4 present the spatial distribution and debris thickness for scenario one with initial slope failure at the toe of the slide in the northern part and in the southern part, respectively at  $t = 30$  min.

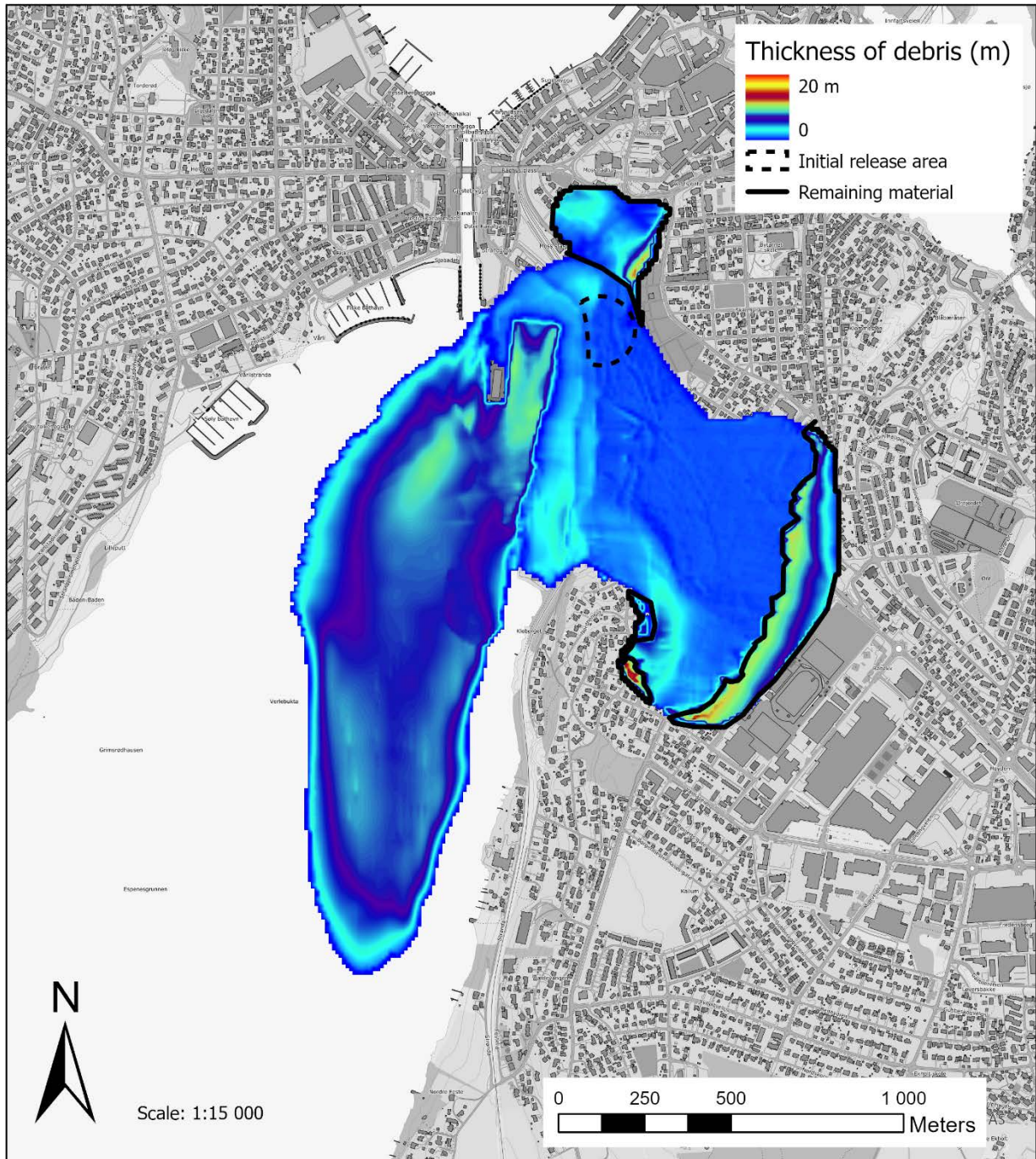


**Figure 3-3 Spatial distribution and debris thickness for scenario one with initial slope failure at the toe of the slide in the northern part of the quick clay zone, as modelled by BingClaw. The initial failure area is indicated with a black dashed line. The area within the solid black line indicates soil masses that are not released into landslide motion.**

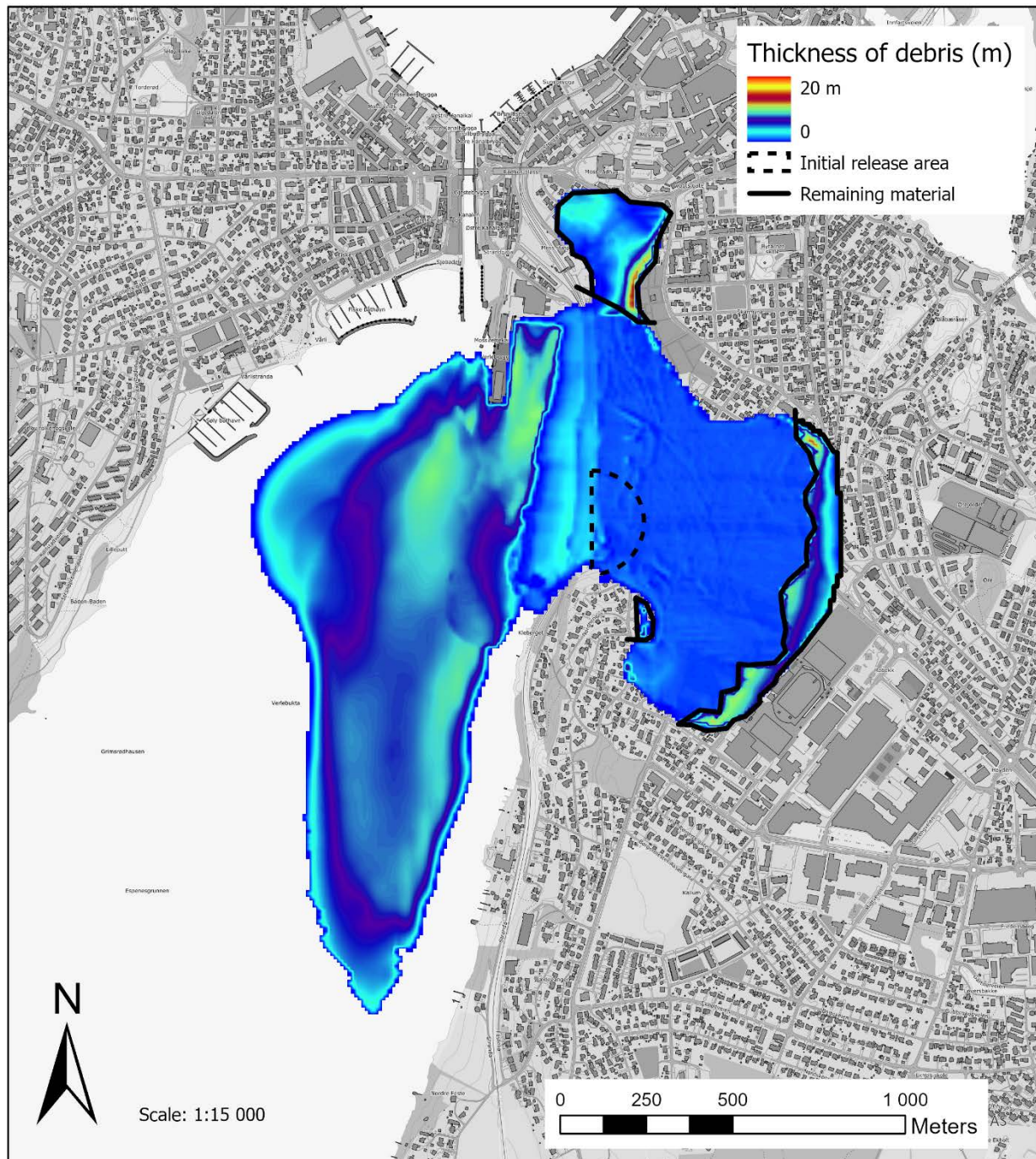


**Figure 3-4 Spatial distribution and debris thickness for scenario one with initial slope failure at the toe of the slide in the southern part of the quick clay zone, as modelled by BingClaw. The initial failure area is indicated with a black dashed line. The area within the solid black line indicates soil masses that are not released into landslide motion.**

<b>BANE NOR</b> Sandbukta-Moss-Såstad	Tsunami Inundation Study	Side: 18 av 32 Dok.nr: SMS-20-A-59615 Rev.: 01C Dato 07.12.2021
--	--------------------------	--

### 3.3 Scenario two

This scenario represents the deepest failure (maximum thickness is around 62 m) and the largest volume (around 17.4 Mm<sup>3</sup>), with higher yield strength values which makes the material less mobile. This scenario uses the following yield strength parameters.

- $\tau_{y,0} = 100$  kPa, and  $\tau_{y,\infty} = 5$  kPa

Figures 3-5 and 3-6 present the spatial distribution and debris thickness for scenario two with initial slope failure at the toe of the slide in the northern part and in the southern part, respectively, at  $t = 30$  min.

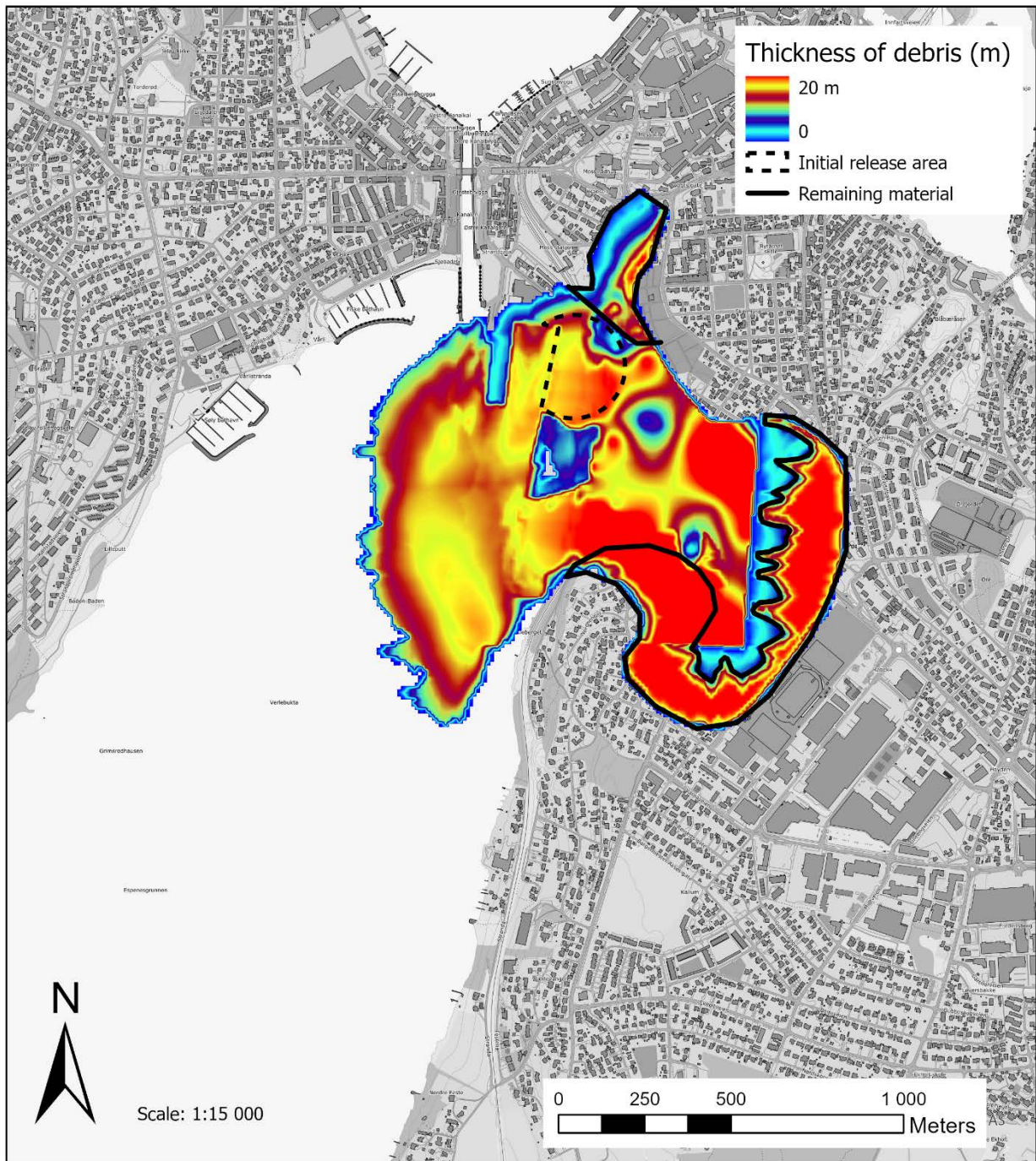


**Figure 3-5 Spatial distribution and debris thickness for scenario two with initial slope failure at the toe of the slide in the northern part of the quick clay zone, as modelled by BingClaw. The initial failure area is indicated with a black dashed line. The area within the solid black line indicates soil masses that are not released into landslide motion.**

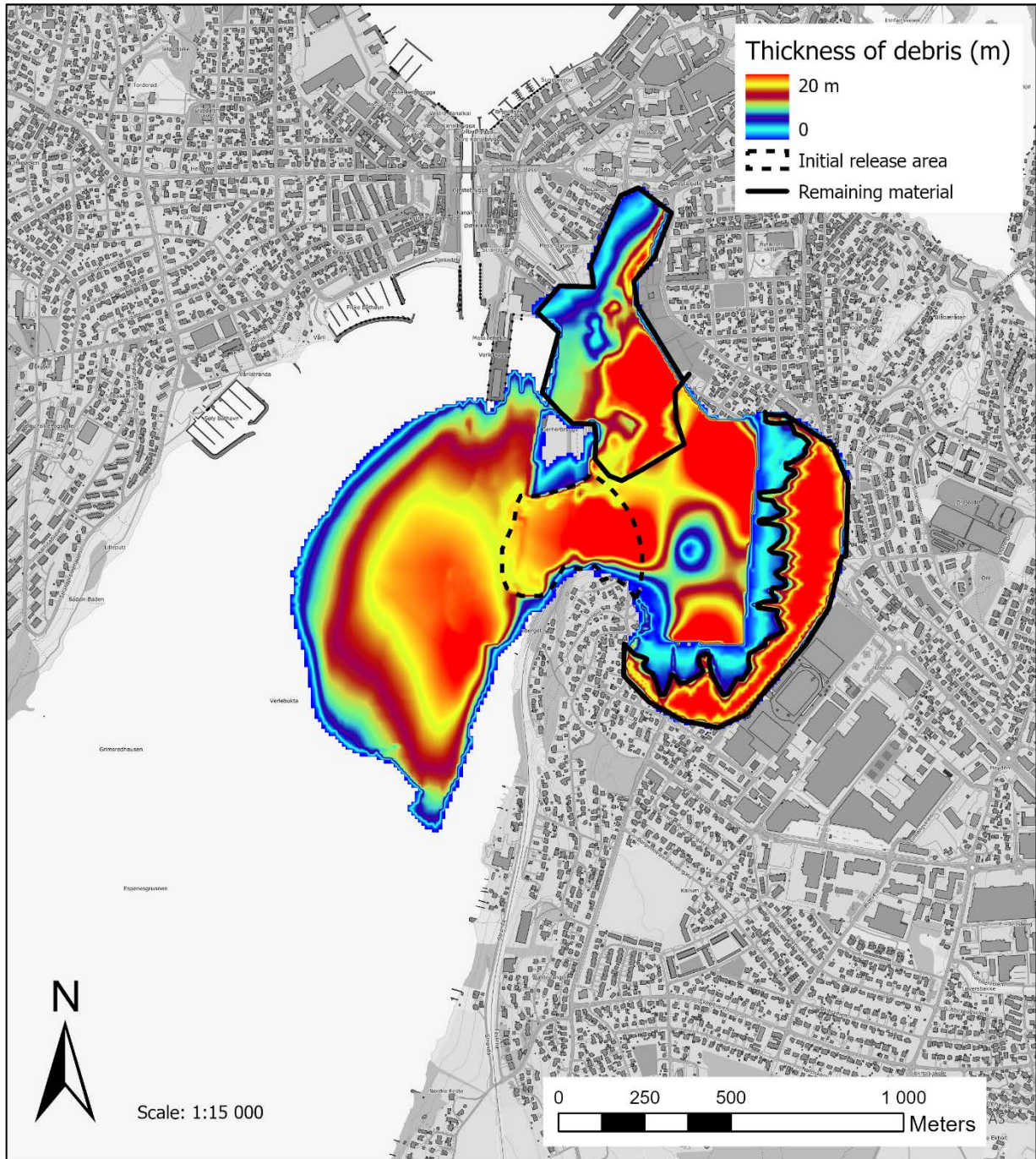


**Figure 3-6 Spatial distribution and debris thickness for scenario two with initial slope failure at the toe of the slide in the southern part of the quick clay zone, as modelled by BingClaw. The initial failure area is indicated with a black dashed line. The area within the solid black line indicates soil masses that are not released into landslide motion.**

<b>BANE NOR</b> Sandbukta-Moss-Såstad	Tsunami Inundation Study	Side: 21 av 32 Dok.nr: SMS-20-A-59615 Rev.: 01C Dato 07.12.2021
--	--------------------------	--

### 3.4 Scenario three

This scenario represents the intermediate failure depth (maximum thickness is around 35 m) and volume (around 15.4 Mm<sup>3</sup>), with intermediate yield strength values. This scenario uses the following yield strength parameters.

- $\tau_{y,0} = 90$  kPa, and  $\tau_{y,\infty} = 3$  kPa

Figures 3-7 and 3-8 present the spatial distribution and debris thickness for scenario three with initial slope failure at the toe of the slide in the northern part and in the southern part, respectively, at  $t = 30$  min.

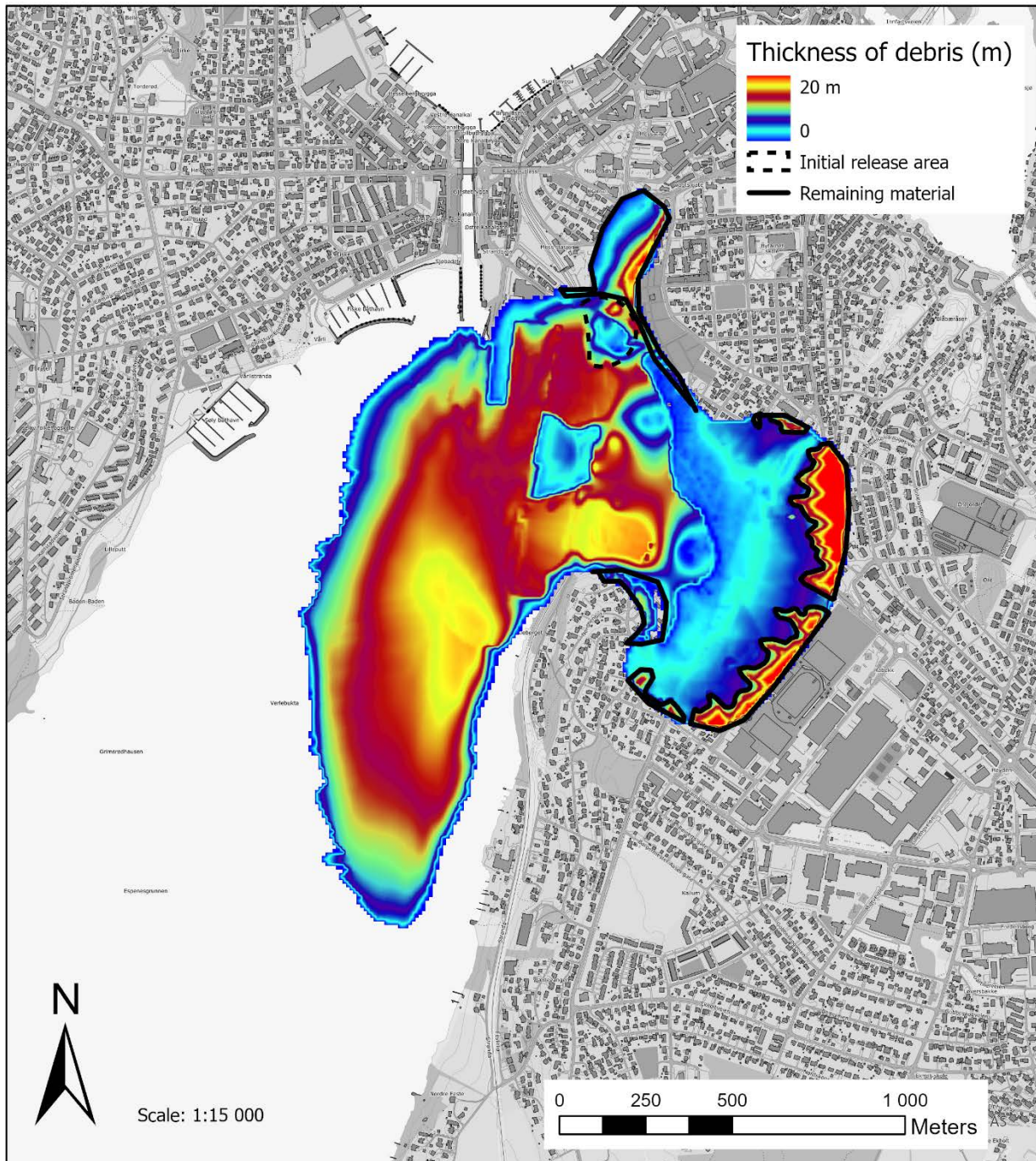


**Figure 3-7 Spatial distribution and debris thickness for scenario three with initial slope failure at the toe of the slide in the northern part of the quick clay zone, as modelled by BingClaw. The initial failure area is indicated with a black dashed line. The area within the solid black line indicates soil masses that are not released into landslide motion.**

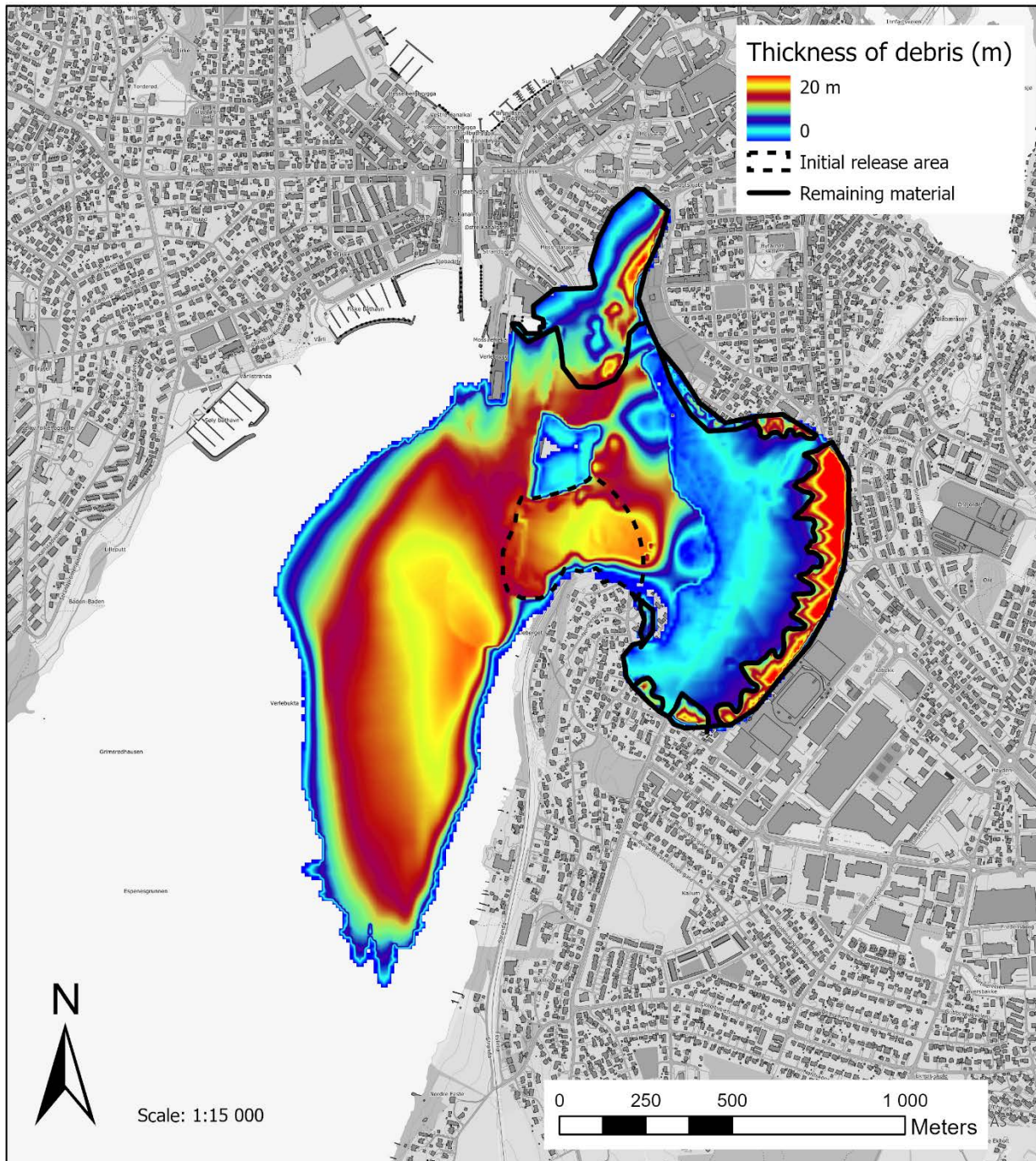


**Figure 3-8 Spatial distribution and debris thickness for scenario three with initial slope failure at the toe of the slide in the southern part of the quick clay zone, as modelled by BingClaw. The initial failure area is indicated with a black dashed line. The area within the solid black line indicates soil masses that are not released into landslide motion.**

<b>BANE NOR</b> Sandbukta-Moss-Såstad	Tsunami Inundation Study	Side: 24 av 32 Dok.nr: SMS-20-A-59615 Rev.: 01C Dato 07.12.2021
--	--------------------------	--

## 4 TSUNAMI PROPAGATION AND INUNDATION

NGI carried out simulations of the tsunami using the Geoclaw model for the tsunami generation, propagation, and inundation. Geoclaw is a well-established tsunami model (of shallow water type) used for a range of different tsunami application worldwide, and it is validated towards existing international tsunami benchmark cases (Gonzalez et al., 2011). In a single model, Geoclaw simulates the tsunami generation from the quick clay landslide and the tsunami propagation in the open sea, as well as the tsunami inundation process. The tsunami generation takes into account the time dependent volumetric displacement of water due to the progressing landslide (using the BingClaw landslide simulations as input).

For the simulations performed here, we combined topographic and bathymetric grids at 5 m resolution shown in Figure 2-4 as input to the wave simulations, including the canal separating Jeløya and mainland, and the Værlebukta bay area south just of the sound. The simulations are aimed towards estimating the inundation in the bay area adjacent to the quick clay zone where the inundation is expected to be highest. Covering a larger area was beyond the scope of this study. A Manning friction parameter of  $n = 0.025$  was used to represent the bottom friction. The simulations were run for 15-30 minutes depending on the duration of the landslide dynamics.

The results for each of the three scenarios are discussed below, presenting contours of the maximum tsunami inundation heights for each of the six tsunami simulations (two different failure areas for each scenario). The contours are extracted from the maximum tsunami inundation heights from the simulations. In addition, an additional 10 m horizontal inundation zone is added to take into account possible uncertainty in the tsunami model.

The results are presented in terms of the maximum inundation heights. The maximum inundation heights are measured as the highest total vertical reach above mean sea level. Other impact metrics such as flow depth and current velocities can also be derived from the analysis, but these are not presented in this report. Tides are not taken into account in the simulations. We remark that in the immediate vicinity of the landslide failure zone, the run-out landslide impact itself and the tsunami inundation is not easily distinguished. In all cases, we remark that the maximum tsunami inundation is generated in the initial part of the landslide motion, implying that the maximum inundation heights are typically generated within 1-5 minutes after the landslide has started to fail. We focus the description of the results on tsunami inundation where the damage potential is assumed to be largest. In addition to this, the tsunami can generate large waves in the sea and strong currents.

### 4.1 Scenario one

The simulated maximum inundation areas for scenario one are shown in Figure 4-1 and Figure 4-2. We assume the initial failure starts in the northern and the southern part of the slope, respectively. Simulated final run-out distances and slope failure areas are also shown in Figure 4-1 and Figure 4-2. Inundation in the southern part is shown in Figure 4-7.

Scenario one produces maximum tsunami inundation heights up to about 3 m, and with moderate horizontal inundation. The horizontal inundation distance (distance from the shoreline to innermost wet point) typically do not exceed 50-60 m on Jeløya, but in addition the tsunami can also overtop several of the local piers. The travel distance from the tip of the largest pier to dry land is significantly longer than this inundation distance. The greatest inundation is generated close to the landslide impact in the ferry harbour area, and on the opposite shorelines just to west of the landslide on Jeløya. The southern failure (Figure 4-2) produces the greatest inundation in distal areas, while the northern failure (Figure 4-1) produces the greatest inundation in the ferry harbour area. The tsunami

can inundate the canal area but is then strongly weakened and not producing significant inundation north of the canal.

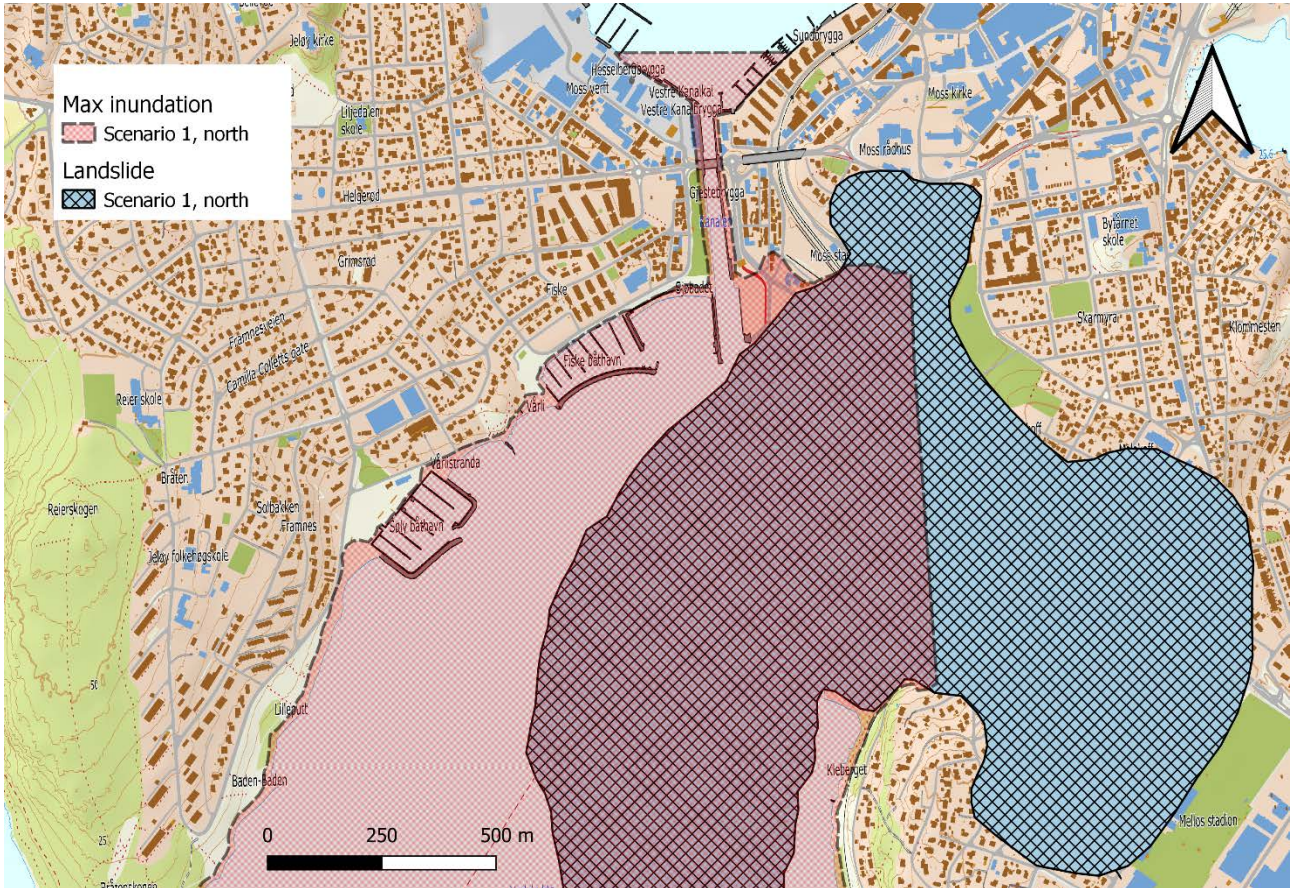


**Figure 4-1** Tsunami inundation zone for scenario one with initial slope failure at the toe of the slide in the northern part of the quick clay zone. The related quick clay failure area and the final modelled run-out distance are indicated with gridlines. In the landslide area the tsunami inundation is less relevant and is also complicated to compute and distinguish from the landslide impact. Therefore, the inundation zone within the landslide area is here marked with a straight line.

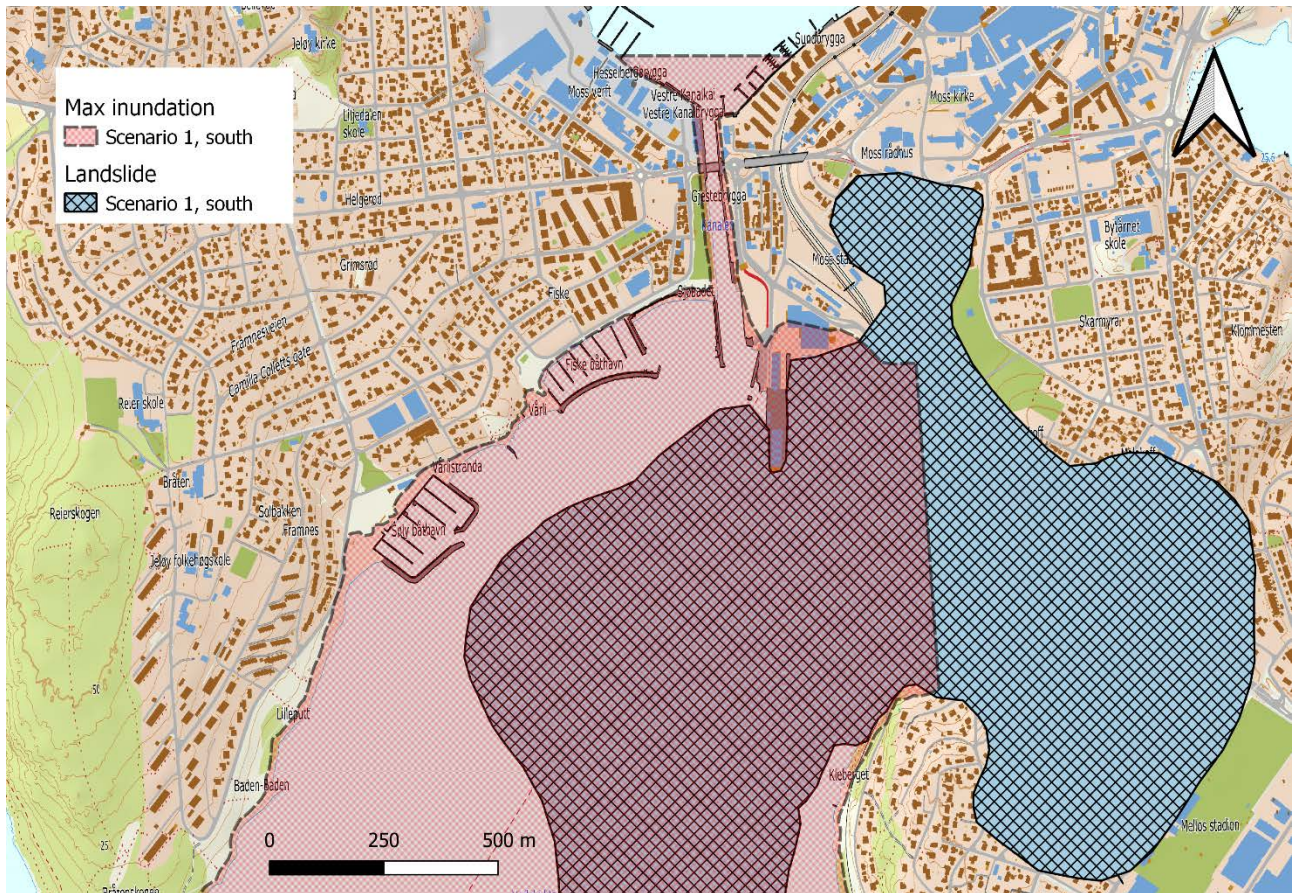


**Figure 4-2** Tsunami inundation zone for scenario one with initial slope failure at the toe of the slide in the southern part of the quick clay zone. The related quick clay failure area and the final modelled run-out distance are indicated with gridlines. In the landslide area the tsunami inundation is less relevant and is also complicated to compute and distinguish from the landslide impact. Therefore, the inundation zone within the landslide area is here marked with a straight line.

## 4.2 Scenario two

The simulated maximum inundation areas for scenario two are shown in Figure 4-3 and Figure 4-4, where we assume the initial failure starts in the northern and the southern part of the slope, respectively. Simulated final run-out distances and slope failure areas are also shown in Figure 4-3 and Figure 4-4. Inundation in the southern part is shown in Figure 4-7.

Scenario two produces maximum tsunami inundation heights up to about 8 m. Thus, scenario two produces greater tsunami inundation than scenario one. The simulated impact differs greatly between the two different failure locations simulated for this scenario, i.e. depending on whether the landslide is initiated in the north or in the south. The horizontal inundation distance (distance from the shoreline to innermost wet point) can extend slightly beyond 100 m on Jeløya, but in addition the tsunami can also overtop several of the local piers. The travel distance from the tip of the largest pier to dry land is significantly longer than this inundation distance. However, we note that greater horizontal inundation distances than 200 m are reached just north of the ferry area for the simulation

assuming initial failure in the northern area. The greatest inundation is generated close to the landslide impact in the ferry harbour area for the northern failure, and on the opposite shorelines just to west of the landslide on Jeløya for the southern failure. The southern failure (Figure 4-4) produces the greatest inundation in distal areas, while the northern failure (Figure 4-3) produces the greatest inundation in the ferry harbour area and northwards. The tsunami can inundate the canal area but is then strongly weakened and not producing significant inundation north of the canal.

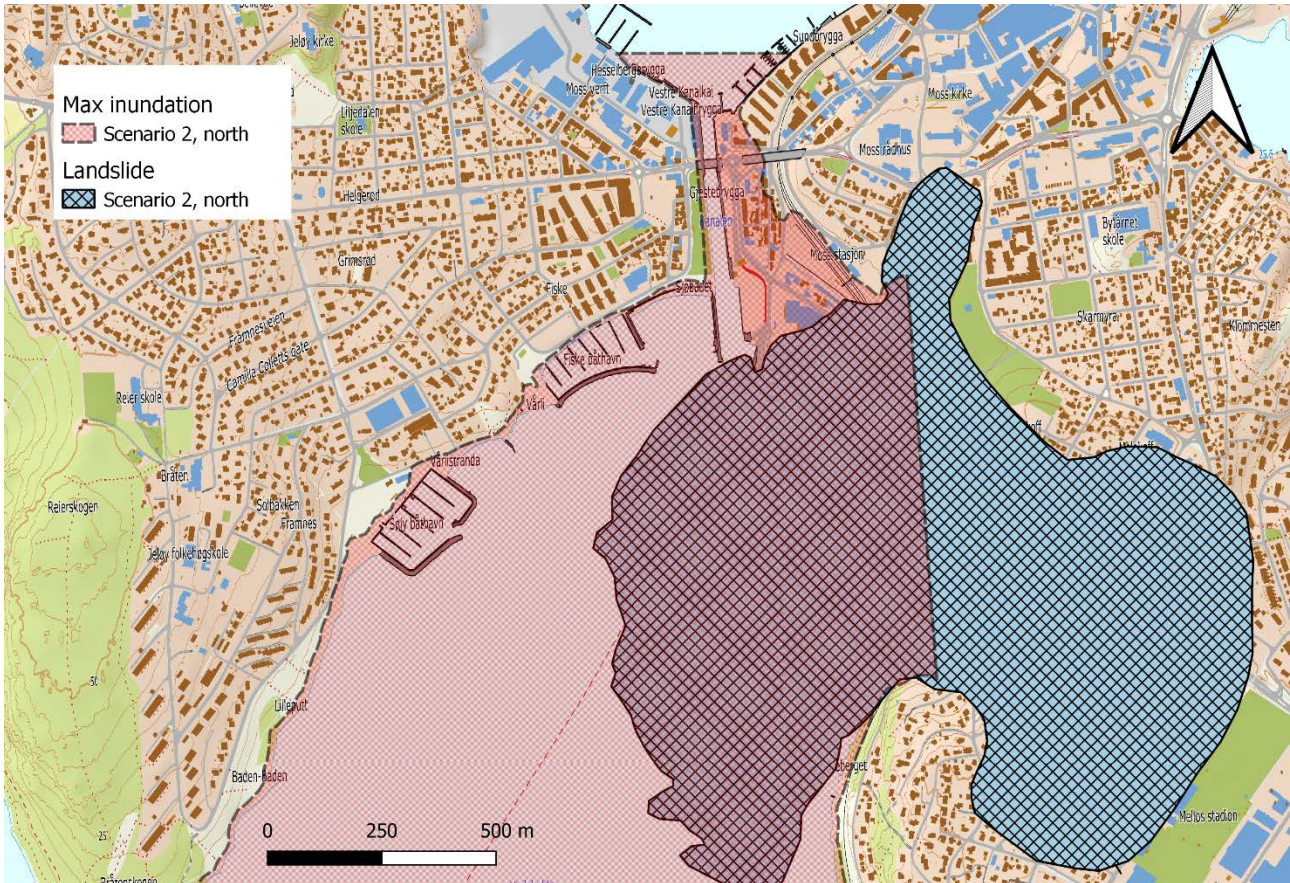


**Figure 4-3 Tsunami inundation zone for scenario two with initial slope failure at the toe of the slide in the northern part of the quick clay zone. The related quick clay failure area and the final modelled run-out distance are indicated with gridlines. In the landslide area the tsunami inundation is less relevant and is also complicated to compute and distinguish from the landslide impact. Therefore, the inundation zone within the landslide area is here marked with a straight line.**



**Figure 4-4 Tsunami inundation zone for scenario two with initial slope failure at the toe of the slide in the southern part of the quick clay zone. The related quick clay failure area and the final modelled run-out distance are indicated with gridlines. In the landslide area the tsunami inundation is less relevant and is also complicated to compute and distinguish from the landslide impact. Therefore, the inundation zone within the landslide area is here marked with a straight line.**

### 4.3 Scenario three

The simulated maximum inundation areas for scenario three are shown in Figure 4-5 and Figure 4-6, where we assume the initial failure starts in the northern and the southern part of the slope, respectively. Simulated final run-out distances and slope failure areas are also shown in Figure 4-5 and Figure 4-6. Inundation in the southern part is shown in Figure 4-7.

The impact of Scenario three is very similar to scenario two. Scenario three produces maximum tsunami inundation heights up to about 7 m. The simulated impact differs greatly depending on the whether the landslide is initiated in the north or in the south. The horizontal inundation distance (distance from the shoreline to innermost wet point) can extend slightly beyond 100 m in the far field, but in addition the tsunami can also overtop several of the local piers. The distance from the tip of the largest pier to dry land is significantly longer. However, we note that greater horizontal inundation distances than 200 m are reached just north of the ferry area for the simulation assuming initial failure in the northern area. The greatest inundation is generated close to the landslide impact in the ferry harbour area for the northern failure, and on the opposite shorelines just to west of the landslide

on Jeløya for the southern failure. The southern failure (Figure 4-6) produces the greatest inundation in distal areas, while the northern failure (Figure 4-5) produces the greatest inundation in the ferry harbour area and northwards. The tsunami can inundate the canal area but is then strongly weakened and not producing significant inundation north of the canal.

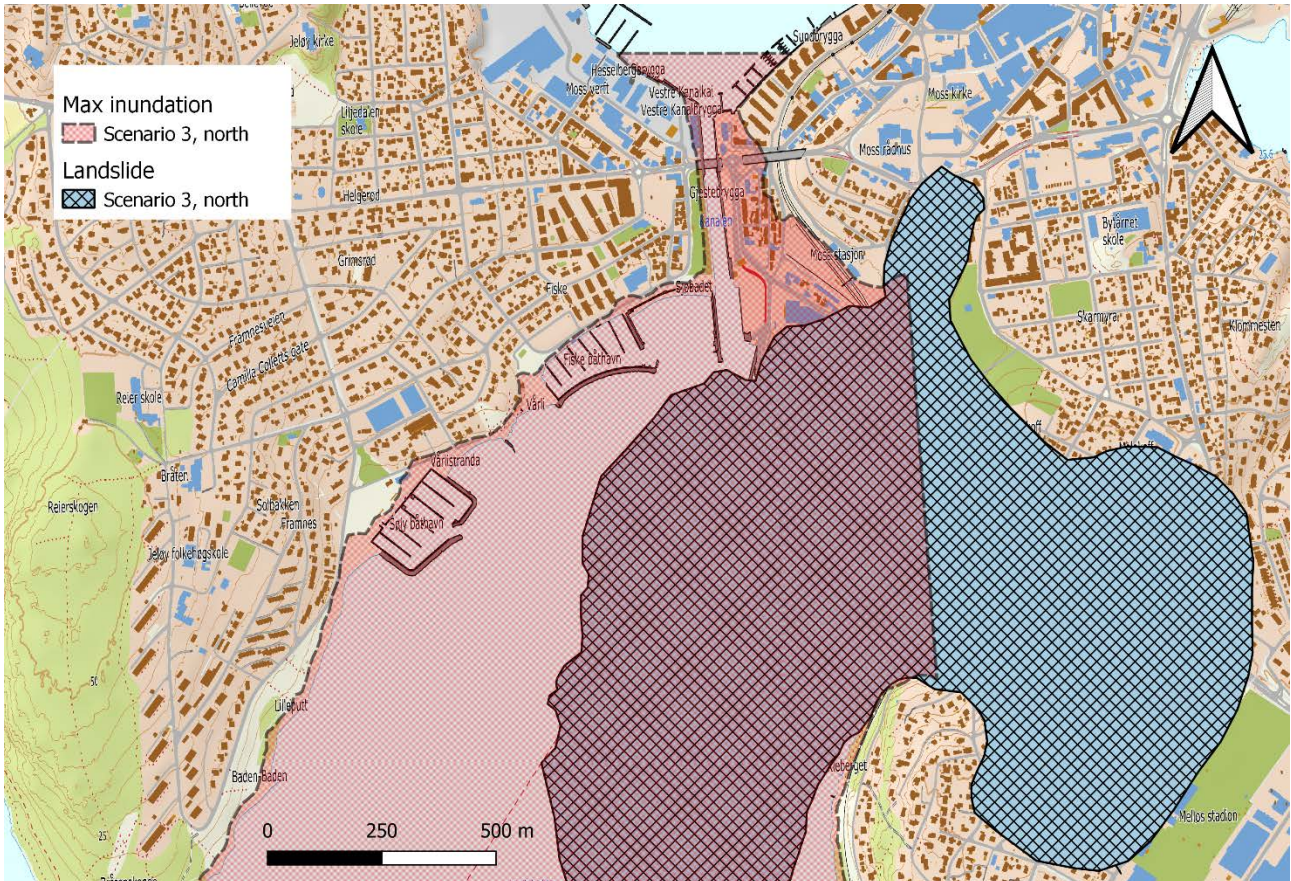


**Figure 4-5 Tsunami inundation zone for scenario three with initial slope failure at the toe of the slide in the northern part of the quick clay zone. The related quick clay failure area and the final modelled run-out distance are indicated with gridlines. In the landslide area the tsunami inundation is less relevant and is also complicated to compute and distinguish from the landslide impact. Therefore, the inundation zone within the landslide area is here marked with a straight line.**

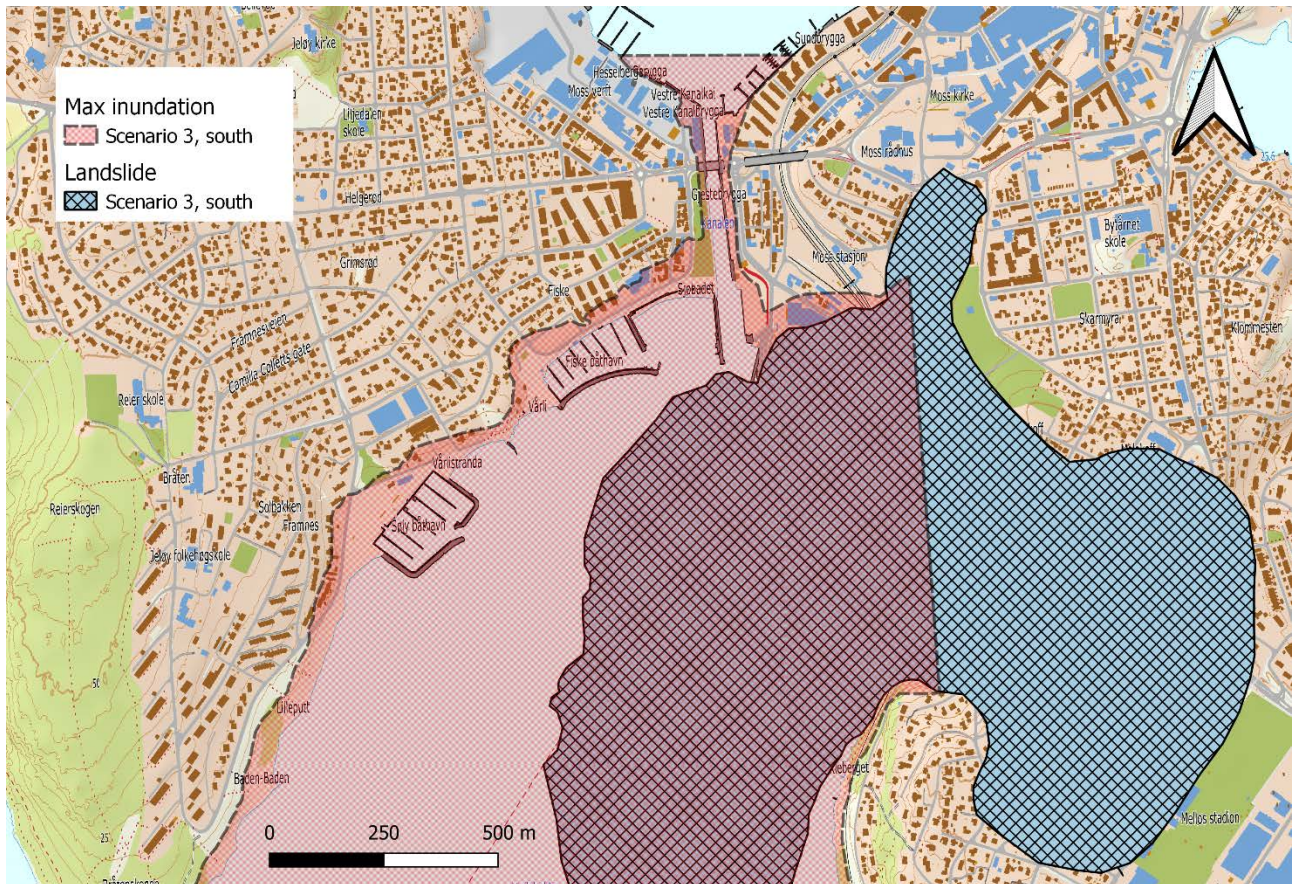


**Figure 4-6 Tsunami inundation zone for scenario three with initial slope failure at the toe of the slide in the southern part of the quick clay zone. The related quick clay failure area and the final modelled run-out distance are indicated with gridlines. In the landslide area the tsunami inundation is less relevant and is also complicated to compute and distinguish from the landslide impact. Therefore, the inundation zone within the landslide area is here marked with a straight line.**



**Figure 4-7 Tsunami inundation zone for scenarios one and three (two is very similar to three and therefore not shown) in the southern part of the simulation domain. The related quick clay failure area and the final modelled run-out distance are indicated with gridlines.**

## 5 CONCLUDING REMARKS

In this report NGI have modelled the tsunami generation from three credible worst-case landslide scenarios where it is assumed that the entire or almost the entire quick clay zone east of the harbour area fails. The probabilities of these worst-case scenarios are not assessed. The different scenarios reflect the uncertainty in the failure depth and location. For each scenario, two simulation examples are provided, one assuming that the failure starts in the north part of the quick clay zone, and the other assuming that the failure starts in the south part of the quick clay zone. Inundation trim lines (contours describing the highest vertical reach of the wave) are simulated for each scenario. The simulations provide the following findings:

- The potentially highest inundations are due to the medium and largest sized volumes (scenarios two and three). These scenarios can give 4-8 m inundation height on the opposite side of the bay in the area surrounding a small boat harbour facility. Large waves are also generated in the vicinity of the landslide failure area. This may potentially imply severely inundation covering a large area between the ferry harbour and the canal west of today's Moss station.
- Scenario one produces lower waves, less than 3 m maximum inundation heights.

<b>BANE NOR</b> <b>Sandbukta-Moss-Såstad</b>	Tsunami Inundation Study	Side: 32 av 32 Dok.nr: SMS-20-A-59615 Rev.: 01C Dato 07.12.2021
---	--------------------------	--

- The scenarios where the failure takes place in the south generates the largest waves towards the opposite shorelines on Jeløya.
- The scenario with initial failure in the north part inundates most severely the area between the harbour area and the canal.
- The tsunami does not propagate with significant strength beyond the canal separating Jeløya and mainland, and is hence restricted to the southern shorelines.
- A limited geographical extent is investigated, see Figure 4-1 - Figure 4-7. It cannot be excluded that significant waves can inundate south and west of the investigated area, but waves are expected to be gradually lower further away from the slope failure area. Studying a larger area was beyond the scope of this study.
- The tsunami inundation trim line can be interpreted as secondary consequences from landslides, and should as such be treated as an elongated run-out zones due to the scenarios investigated.

## 6 REFERENCES

- González, F. I., LeVeque, R. J., Chamberlain, P., Hirai, B., Varkovitzky, J., and George, D. L. (2011). Validation of the geoclaw model. In NTHMP MMS Tsunami Inundation Model Validation Workshop. GeoClaw Tsunami Modeling Group.
- Kim, J., Løvholt, F., Issler, D., and Forsberg, C. F. (2019). Landslide material control on tsunami genesis — the Storegga Slide and tsunami (8,100 years BP). *Journal of Geophysical Research: Oceans*, 124(6), 3607-3627.
- Liu Z.Q., Lacasse S., Nadim F., L'Heureux J.S., Kim J., Thakur V. (2018). Modelling of landslide runout in sensitive clays. *Proc. Geohazards 7*. Canmore, Canada.
- NGI (2021). Østfoldbanen VL, Sandbukta – Moss – Såstad, Km 56,075 – 66,410, Vurdering av områdestabilitet. NGI report 20190539-11-R, revision 4, 2021-01-29. Bane NOR project number 960168, document number SMS-00-A-590002, revision 00E.
- NVE (2020). Ekstern rapport nr. 9/2020. Oversiktskartlegging og klassifisering av faregrad, konsekvens og risiko for kvikkleireskred. Metodebeskrivelse, NGI.
- Sinding-Larsen E. Runout modelling. Strain-softening of landslide debris. MSc thesis, NTNU Norwegian University of Science and Technology. June 2019. 67 pp.